

# Power Beacon Placement for Maximizing Guaranteed Coverage in Bistatic Backscatter Networks

Xiaolun Jia, *Student Member, IEEE*, and Xiangyun Zhou, *Senior Member, IEEE*

## Abstract

The bistatic backscatter architecture enables flexible deployment opportunities for backscatter devices by extending communication range. In this paper, we study the placement of power beacons (PBs) in bistatic backscatter networks to maximize the guaranteed coverage distance (GCD), defined as the distance from the reader within which the backscatter devices are able to satisfy a given quality-of-service constraint. This work departs from conventional energy source placement problems by considering the performance of the additional backscatter link on top of the energy transfer link. We adopt and optimize a symmetric PB placement scheme to maximize the GCD. The optimal PB placement under this scheme is obtained using either analytically tractable expressions or an efficient algorithm. Numerical results provide useful insights into the impacts of various system parameters on the PB placement and the resulting GCD, plus the advantages of the adopted symmetric placement scheme over other benchmark schemes.

## Index Terms

Bistatic backscatter communication, coverage, placement optimization, power beacons.

## I. INTRODUCTION

### A. Background

The Internet-of-Things (IoT) paradigm has brought renewed research interest in the area of low-power communication, given the improved capabilities of wireless sensors and their potential for use in pervasive networking and monitoring. Low-power sensors have traditionally found uses in environmental monitoring, where sensed data obtained over certain geographical areas are transmitted to a central receiver. So far, the majority of existing sensing devices perform active

transmissions, which consume significant power and hence limit the lifetime of battery-powered devices.

Backscatter communication has emerged as a promising technology to improve device lifetime. Communication is performed passively using the energy available in existing radiofrequency (RF) signals rather than by generating new signals using active transmit chains, thus significantly reducing the overall power consumption. A prime example of the backscatter paradigm is radiofrequency identification (RFID), in which a powered reader transmits an unmodulated continuous wave (CW) signal, which is received by an RFID tag. The tag then modulates its data onto the CW by switching between load impedances connected to its antenna to change the amount of reflected signal power, and the modulated signal returns to the reader to be decoded. Some notable studies on RFID system performance can be found in [1]–[3].

Among the different backscatter architectures, the bistatic architecture, whose concept can be traced back to [4], has received considerable recent interest. It consists of an RF carrier emitter separate from the reader, which allows improved ranges due to non-correlated fading in the power-up and backscatter links. Link budgets for the bistatic architecture were studied in detail in [5]. Initial communication-theoretic and experimental studies using commodity radios were conducted by the authors of [6], where communication ranges of over 100 m were achieved — an order of magnitude further than that achieved in the monostatic and ambient architectures. Much subsequent effort was devoted to range improvement, to take advantage of the lower cost to deploy PBs over readers. Channel coding and interleaving at the BD were examined in [7] to mitigate the effect of deep fades, in addition to various coherent detectors, where ranges of up to 150 m were demonstrated; while work in [8] proposed solutions to the phase cancellation problem experienced when unmodulated carriers are used. Work in [9] extended [7] to account for noncoherent detection and considered the scenario where the BD transmits short packets typical of IoT devices; while work in [10] took advantage of the separation of reader and PB and introduced a grant-free random access protocol for BDs.

### *B. Bistatic Backscatter and Energy Source Placement*

Much research has focused on single-user backscatter communication; however, few works have studied system-level performance analysis of backscatter networks, with one category being coverage characterization based on how the PBs are deployed. Range measurements in [6] suggested that the coverage areas of PBs have irregular shapes, depending on the location of a

PB relative to the reader. Work in [11] utilized stochastic geometry to model the deployment of collocated readers and PBs, where BDs were clustered around each reader, and analyzed metrics including coverage and transmission capacity. Work in [12] compared the performance of a bistatic network with multiple PBs to a monostatic system. A square-grid PB placement scheme was considered; although an optimal PB placement to maximize coverage was not examined. Work in [13] considered a similar setup as [11] and compared coverage and capacity to a non-backscatter wireless-powered communication network (WPCN). However, it assumed random PB locations and D2D communication between BDs, as opposed to BD-reader communication, and used a stochastic geometry approach rather than a deterministic PB placement scheme.

Some similarities exist between the PB placement problem and the relay placement problem in conventional communications, with representative studies in [14]–[17]. Often, the aim is to determine the optimal position of a powered relaying node to satisfy coverage, throughput or lifetime constraints for distantly located nodes. It is known that finding an optimal placement for relays fulfilling such constraints is intractable [14], [16]; thus, works such as [17] resorted to algorithms that guarantee solutions with various approximation ratios. However, in the context of backscatter networks, PBs are different from relaying nodes when coverage is concerned. This is due to the fully coupled nature of PB-BD and BD-reader communications under backscattering, as opposed to the mostly decoupled source-relay and relay-destination communications in the relaying networks, where the ‘coverage areas’ of relay nodes tend to be circular.

The other technology utilizing PBs is WPCNs [18]–[20], wherein users harvest and store energy received from RF sources for use in active transmissions. Studies on energy source placement in WPCNs include [21]–[27]. Specifically, [21] considered a symmetric deployment of PBs equidistant from a base station, and derived closed-form outage probability expressions in terms of the number of PBs and their distance from the base station. Work in [26] studied a symmetric placement scheme for the distributed antennas of PBs, and established the optimal antenna locations that maximized the wireless power transfer efficiency. Both works assumed users located at uniformly random locations. On the other hand, work in [22] assumed known user locations and proposed suboptimal algorithms to divide the network area into partitions, where one PB was deployed at a time to ensure that each PB and all PBs beforehand were placed in locally-optimal locations. While such proposals are able to benefit communication performance in conventional wireless-powered networks, the signal model for backscatter communication is considerably different from that of WPCNs, and a different analysis approach is required to

account for the complete dependence of BDs' communications on external RF signals.

### *C. Motivation and Contributions*

We note that apart from a small number of exceptions such as [21], [27], existing works on energy source placement in conventional wireless-powered networks have examined scenarios where the PB locations are selected according to a specific user topology. Moreover, none of the works discussed in Section I-B are applicable to bistatic backscatter networks, which constitutes a significant knowledge gap. For backscatter networks, the BDs are often small-size, low-cost devices, while PBs are much more costly. Hence, it is often reasonable to determine PB placement prior to BD deployment so that the locations of some BDs can be changed from time to time. As a result, it is worth determining a PB placement strategy that aims to provide coverage over a targeted geographical area, rather than a specific set of BD deployment locations.

In this paper, we consider the deterministic placement of PBs in a bistatic backscatter network, where a reader (i.e., the data collection unit) is centrally located in a geographical area where BDs are to be deployed. To the best of our knowledge, the placement of PBs in a bistatic backscatter network is yet to be addressed in the literature. We study the placement of PBs to maximize the distance from the reader within which BDs are guaranteed to meet a certain quality-of-service (QoS). That is, our PB placement design guarantees the coverage of BDs based on their distances from the reader, instead of their specific locations. This enables the BD topology to be altered without requiring redeploying PBs (for which significant effort is required), which can be beneficial for wide-area environmental monitoring, inventory tracking and localization, where large numbers of BDs are present over a certain geographical area, and whose locations may be subject to changes. The problem is unique in that the coverage areas of individual PBs are irregularly shaped, owing to the asymmetric nature of the PB-BD and BD-reader links under bistatic backscatter. Our main contributions are as follows:

- We present the first study on the PB placement problem in bistatic backscatter networks. By defining the QoS in terms of an outage probability constraint, we formulate the PB placement problem for maximizing the guaranteed coverage distance (GCD), a metric which we propose for its straightforward characterization of the coverage area.
- Due to the intractable nature of solving for the optimal PB placement, we adopt a circular symmetric placement strategy that is commonly used in conventional WPCNs. We examine cases where each BD is served either by its nearest PB or simultaneously by multiple nearest

PBs. Closed-form expressions for the optimal PB-reader distance and asymptotic GCD are derived for the case where each BD is served by its nearest PB; and a low-complexity algorithm is proposed to determine the optimal PB-reader distance when multiple serving PBs are involved.

- Extensive numerical results are presented to characterize the impacts of system parameters on the GCD, and to highlight design insights. Particularly, a significant GCD improvement is observed by using two serving PBs for each BD instead of only one serving PB, but allowing more than two serving PBs quickly results in diminished returns. Comparisons with alternative PB placement schemes are also presented, which highlight the favorable performance of our placement scheme given its low-complexity nature.

The rest of this paper is organized as follows. Section II introduces the system and signal models, and formulates the PB placement problem. Section III derives the BD outage probability and presents the solution to the PB placement problem, for the case where each BD is served by its nearest PB. Section IV presents a low-complexity algorithm for solving the PB placement problem where each BD is served by multiple PBs. Numerical results are presented in Section V and Section VI concludes the paper.

*Notations:*  $j = \sqrt{-1}$  denotes the complex unit, and  $|\cdot|$  denotes the magnitude of a complex number.  $\mathbb{E}\{\cdot\}$  and  $\Pr(\cdot)$  denote the expectation operator and the probability of an event, respectively.  $\Gamma(\kappa, \tau)$  denotes a gamma random variable with shape parameter  $\kappa$  and scale parameter  $\tau$ . Boldface letters denote vectors, as in  $\mathbf{a}$ ;  $\|\mathbf{a}\|$  denotes the Euclidean norm of  $\mathbf{a}$ .

## II. SYSTEM MODEL AND PROBLEM FORMULATION

We consider a bistatic backscatter network with one reader located at the origin and a number of BDs dispersed around the reader. The BDs are assumed to be stationary, but their locations within the network may change in the long term for application-specific purposes. The data packets generated at the BDs are to be transmitted to the reader via backscattering. We assume semi-passive BDs with built-in batteries to support their circuit operations, and extend the analysis numerically to passive BDs with a circuit power constraint in Section V-C. Each BD has two load impedances connected to its antenna. Two modulation schemes are commonly considered in bistatic backscatter networks, namely on-off keying (OOK) and frequency-shift keying (FSK). Where OOK is used, we assume that one BD is served at a time — that is, the BD being served needs to be acknowledged by the network through a contention process before transmission can

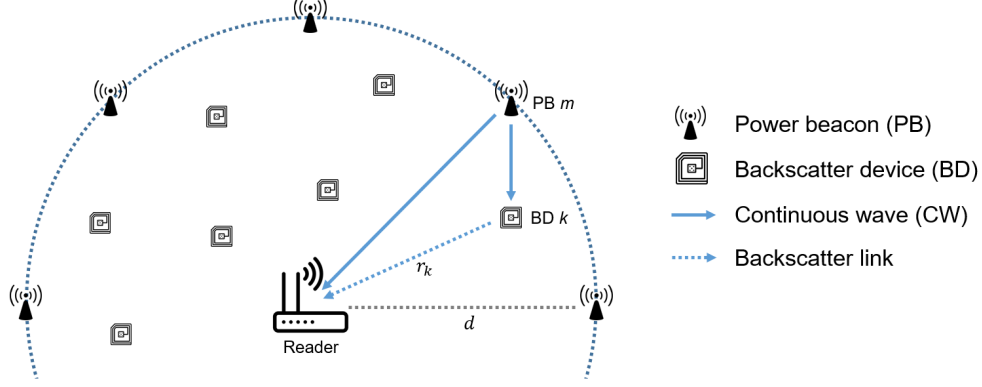


Fig. 1: Bistatic backscatter network with PBs.

occur. Where FSK is used, multiple BDs may simultaneously backscatter their data symbols using unique, sufficiently spaced subcarrier frequencies assigned to each BD. Since no interference occurs between the backscatter transmissions from the BDs in either case, we focus our analysis on a single BD. We show in the sequel that the coverage analysis for both modulation schemes can be performed using an identical procedure.

A total of  $M$  PBs are to be deployed to facilitate the backscatter communication of the BDs. The PBs perform energy transmissions omnidirectionally [22], [27] with equal transmit powers denoted by  $P$ . We allow either one or multiple nearest PBs to serve a BD (e.g., two PBs can simultaneously provide energy transmissions to serve the same BD). The set of indices of the PBs serving BD  $k$  is denoted by  $\Phi_k$ .

For the rest of this paper, we abbreviate PBs (a.k.a. carrier emitters), BDs (a.k.a. tags) and the reader as  $C$ ,  $T$  and  $R$ , respectively, in boldface letters and subscripts. Indexing for PBs and BDs are  $m \in \{0, \dots, M-1\}$  and  $k \in \{1, \dots, K\}$ . The system diagram is shown in Fig. 1.

#### A. Channel Model

Denote the complex channel coefficient from node  $i$  to node  $j$  by  $h_{i,j}$ , which accounts for small-scale fading such that

$$\mathbb{E}\{|h_{i,j}|^2\} = \beta_0 \|\mathbf{n}_i - \mathbf{n}_j\|^{-\delta}, \quad (1)$$

where  $\beta_0 = \left(\frac{\lambda}{4\pi}\right)^2$  is the reference path loss;  $\lambda$  is the carrier wavelength;  $\delta \geq 2$  is the path loss exponent; and  $\mathbf{n}_k$  is the coordinate vector of node  $k$  of type  $\mathbf{n} \in \{\mathbf{c}, \mathbf{t}, \mathbf{r}\}$  for PB, BD

and reader, respectively. Frequency-flat quasi-static fading is assumed, consistent with existing backscatter works. In this paper, we adopt Nakagami small-scale fading due to its mathematical tractability, as in [12], [28], and also for its ability to approximate line-of-sight situations, which is common for the applications of bistatic backscatter considered in [6], [9], [12]. We assume uniform propagation conditions throughout the network, noting that the nonuniform case (e.g., localized blockages) is another important problem, but is outside the scope of this work.

### B. Signal Model

Each serving PB transmits an identical CW signal with power  $P$ . The equivalent baseband signal received at BD  $k$  from the serving PB set is the superposition of all the CW components:

$$y_k(t) = \sqrt{P} \sum_{m \in \Phi_k} h_{C_m, T_k} c(t), \quad (2)$$

where  $c(t)$  is the baseband representation of the CW. BD  $k$  performs modulation on the CW by switching between its two impedances to generate two reflection coefficients, which determine the strength of the backscattered signal. The baseband information signal at BD  $k$  is given by

$$b_k(t) = A_k - G_k(t), \quad (3)$$

where  $A_k \in \mathbb{C}$  is the antenna structural mode of BD  $k$ , and  $G_k(t) \in \mathbb{C}$  refers to the time-varying reflection coefficient function.  $G_k(t)$  takes on two values  $G_{k,0}$  and  $G_{k,1}$ , with unit magnitude or less. This results in two values for  $b_k(t)$ , denoted by  $b_{k,0}$  and  $b_{k,1}$ . The backscattered signal is

$$x_k(t) = \sqrt{\eta} y_k(t) b_k(t), \quad (4)$$

where  $\eta$  is the backscatter switching loss coefficient, herein modeled as a constant that is consistent across all BDs. Note that no noise term is present in  $x_k(t)$ , which is a common assumption in the backscatter literature, as BDs do not perform any signal processing. The reader receives the summation of the backscattered information signal and a direct-link CW signal, in addition to the noise.

We first derive the per-symbol SNR at the reader for a symbol transmitted by the BD under OOK. The received signal can be written as

$$x_R(t) = \sqrt{P} \sum_{m \in \Phi_k} h_{C_m, R} c(t) + \sqrt{P\eta} h_{T_k, R} b_k(t) \sum_{m \in \Phi_k} h_{C_m, T_k} c(t) + w(t), \quad (5)$$

where  $w(t)$  is the noise at the reader. The first term in (5) is a constant term due to the direct-link CW, while the second term switches between two levels due to the  $b_k(t)$  term. We assume that

the reader is able to cancel the DC term in (5), and first drop the direct link term [6]. The second term in (5) can then be rewritten as the average of the two levels caused by  $b_k(t)$ , and a modulated component, as follows:

$$\tilde{x}_R(t) = \left( \sqrt{P\eta} h_{T_k,R} \sum_{m \in \Phi_k} h_{C_m,T_k} c(t) \right) \left( \frac{b_{k,0} + b_{k,1}}{2} + \frac{b_{k,0} - b_{k,1}}{2} \mathcal{B}(t) \right) + w(t), \quad (6)$$

where  $\mathcal{B}(t) \in \{-1, 1\}$ , representing the two levels. Note that  $\frac{b_{k,0} + b_{k,1}}{2}$  is also a DC term and can be removed. Following the removal of both DC terms, the received signal at the reader is discretized with sampling period  $T$ , which results in two possible values for the received signal:

$$x_R[l] = \pm \left( \sqrt{P\eta} h_{T_k,R} \sum_{m \in \Phi_k} h_{C_m,T_k} c(lT) \right) \frac{b_{k,0} - b_{k,1}}{2} + w[l]. \quad (7)$$

We let each symbol period  $T_{sym}$  be comprised of  $L$  samples, i.e.,  $T_{sym} = LT$ .

Under OOK, the reflection coefficient  $b_k[l]$ , in the form of  $b_{k,0}$  and  $b_{k,1}$  in (7), remains constant over  $L$  samples of one symbol. Let  $p$  and  $q$  represent the non-noise term in the two quantities in (7), with  $i = 0$  and  $1$ , respectively. That is,  $p = - \left( \sqrt{P\eta} h_{T_k,R} \sum_{m \in \Phi_k} h_{C_m,T_k} \right) \frac{b_{k,0} - b_{k,1}}{2}$  and  $q = \left( \sqrt{P\eta} h_{T_k,R} \sum_{m \in \Phi_k} h_{C_m,T_k} \right) \frac{b_{k,0} - b_{k,1}}{2}$ . In defining the SNR, the ‘signal’ term is given by the difference between  $|q|$  and  $|p|$ . Setting  $|p|$  as the reference level, we take  $(|q| - |p|)^2$  as the signal energy and obtain the following expression for the SNR, defined over one symbol period, in a similar manner compared to [6]:

$$\gamma_k = \frac{(|q| - |p|)^2}{N_0} L = \frac{P\eta |h_{T_k,R}|^2 |b_{k,0} - b_{k,1}|^2 \left| \sum_{m \in \Phi_k} h_{C_m,T_k} \right|^2}{N_0} L, \quad (8)$$

where  $N_0$  is the variance of the discrete-time noise samples  $w[l]$ .

Now we consider FSK modulation. In this case, switching between the two signal levels, similar to those in (7), occurs over each symbol period at one of two subcarrier frequencies denoted by  $f_{k,0}$  and  $f_{k,1}$  for the  $k$ -th BD, which represent bits 0 and 1, respectively. Thus, the discretized baseband signal at the reader, after removing the DC terms, is given as [6, Eq. (52)]

$$x_R[l] = \left( \sqrt{P\eta} h_{T_k,R} \sum_{m \in \Phi_k} h_{C_m,T_k} \right) \frac{b_{k,0} - b_{k,1}}{2} \text{SW}(i, lT) + w[l], \quad (9)$$

where  $\text{SW}(i, t) = \frac{4}{\pi} \cos(2\pi f_i t + \phi)$  is the baseband representation for a square wave with 50% duty cycle, frequency  $f_i$  and filtered at the fundamental frequency, with  $\phi \in [0, 2\pi]$  and  $i \in \{0, 1\}$ . As the cosine term oscillates between  $-1$  and  $1$ , the two signal levels, similar to  $p$  and  $q$  before, are given by  $\pm \left( \sqrt{P\eta} h_{T_k,R} \sum_{m \in \Phi_k} h_{C_m,T_k} \right) \frac{2(b_{k,0} - b_{k,1})}{\pi}$ . Notice that the received signal



under FSK has an additional  $\frac{2}{\pi}$  term compared to OOK, and that the two signal levels apply to both bits 0 and 1, with the two symbol representations differing only in the frequencies of their CW representations at baseband. The signal is demodulated using a correlator demodulator set to frequencies  $\pm f_{k,0}$  and  $\pm f_{k,1}$ , where, if bit 0 is sent, the demodulator at  $\pm f_{k,0}$  outputs magnitude equal to (9), while the demodulator at  $\pm f_{k,1}$  outputs the noise power, and vice versa. The per-symbol SNR is similarly defined as in [6] by

$$\gamma_k = \frac{4P\eta |h_{T_k,R}|^2 |b_{k,0} - b_{k,1}|^2 \left| \sum_{m \in \Phi_k} h_{C_m,T_k} \right|^2}{\pi^2 N_0} L. \quad (10)$$

Thus, we find that the SNR definition under FSK takes on an equivalent form compared to that of OOK in (8), differing only by a multiplicative constant of  $\frac{4}{\pi^2}$ . This means that the SNR-based analysis and design for both OOK and FSK are essentially the same (with a slight difference in the interpretation of results due to the multiplicative constant). Hereafter, we will use (8) as the SNR definition in our analysis and design.

We note the existence of several additional parameters in the link budget of bistatic backscatter communication, as outlined in [5], such as antenna gains, polarization mismatch and on-object gain penalties, which can be readily added to the numerator or denominator of the SNR for gains and losses, respectively.

### C. Performance Metric and Problem Formulation

In this work, we aim to address the PB placement problem for maximizing the coverage area of the network. The metric we use to represent coverage is the GCD, denoted by  $r_{cov}$ . Given a reader at the center of the network, the GCD is defined as the maximum distance at which a BD can be located from the reader, such that it is able to achieve a given QoS requirement. In other words, any BD located at a distance smaller than  $r_{cov}$  from the reader is guaranteed to achieve the QoS requirement. The QoS is indicated by the outage probability, given for BD  $k$  by  $P_{out,k} = \Pr(\gamma_k < \gamma_{th})$ , where  $\gamma_{th}$  is the minimum acceptable SNR threshold. The QoS requirement is then given by a maximum acceptable outage probability, denoted by  $\varepsilon$ . In other words, if BD  $k$  is located at a distance smaller than  $r_{cov}$ , it is guaranteed to have  $P_{out,k} < \varepsilon$ .

The problem considers the placement of  $M$  PBs in carefully chosen locations to maximize the GCD. In general, finding the optimal PB placement is analytically intractable and typically requires exhaustive search. To facilitate the network design, we consider one placement scheme that deploys the PBs at equal distance  $d$  from the reader, with equal angular separation, similar

to prior works on wireless power transfer such as [21], [26], [27]. Different to these works, however, the additional backscatter link must also be accounted for in the coverage analysis. We numerically demonstrate the favorable performance of this placement strategy compared to other schemes in Section V-D. We aim to determine the optimal PB-reader distance,  $d^*$  (hereafter referred to simply as ‘PB distance’), such that  $r_{cov}$  is maximized.

The considered scheme is independent of specific BD locations (i.e., the design of  $d^*$  is not specifically optimized for any BD topology), such that BDs can be installed, removed or relocated without requiring the PBs to be redeployed. A further important consideration in our placement strategy is to guarantee no coverage holes, i.e., all locations within distance  $r_{cov}$  of the reader must satisfy the QoS requirement, which renders random (as opposed to deterministic) placement schemes inappropriate for this purpose. Coverage holes occur when the PB-reader distance is large, causing the coverage area to become discontinuous. To avoid coverage holes, and to ensure ease of BD deployment without the need to manually verify coverage at every location, it is necessary to impose a QoS requirement at all locations. The use of the GCD distinguishes our problem compared to e.g., [21], which performs the placement optimization by averaging the outage probability over the entire network without guaranteeing a minimum QoS requirement at every location.

The problem can be written as (Problem **P1**):

$$\max_d \quad r_{cov}(\{\mathbf{c}_i\}, \{\mathbf{t}_k\}) \quad (11a)$$

$$\text{s.t.} \quad P_{out,k} < \varepsilon, \forall k : \|\mathbf{t}_k\| < r_{cov}, \quad (11b)$$

$$\|\mathbf{c}_i\| = d, \forall i \in \{1, \dots, M\}, \quad (11c)$$

$$\theta_{m_i, m_j} = \frac{2\pi}{M} \quad \forall i, j : i \in \{0, \dots, M-1\}, j \in \{i-1, i+1\} \bmod M, \quad (11d)$$

where  $\{\mathbf{c}_i\}$  and  $\{\mathbf{t}_k\}$  denote the sets of PB and BD location vectors; and  $\theta_{m_i, m_j} = \theta_{m_i} - \theta_{m_j}$  represents the angular spacing between adjacent PBs  $i$  and  $j$ . Constraint (11b) states that all BDs within the GCD must satisfy the QoS requirement; (11c) requires that all PBs must be equidistant from the reader; and (11d) requires equal angular spacing between adjacent PBs. Problem **P1** is complicated by the fact that an expression for  $r_{cov}$  is not available beforehand. To address this significantly limiting factor and to improve mathematical tractability, in the following sections, we solve an equivalent problem, and in the process, obtain insights into the behavior of  $r_{cov}$ .

Hereafter, we drop the BD indexing and focus on one representative BD. In the following sections, we will separately analyze the cases of single and multiple serving PBs.

### III. PB PLACEMENT ANALYSIS: SINGLE SERVING PB

In this section, we analytically derive the optimal PB placement distance when each BD is served only by its nearest PB. First, the exact outage probability expression for an arbitrarily located BD is presented, in terms of its distance from the reader  $r$  (to refer to the communication range of BDs), the PB distance  $d$ , and the number of PBs  $M$ . We then solve the PB placement problem based on our proposed placement scheme, and provide exact expressions for  $d^*$ . For ease of exposition, we denote all distance quantities associated with a PB's location by the variable  $d$  and associated subscripts, and assign the variable  $r$  and associated subscripts to describe the location for an arbitrary BD.

#### A. Outage Probability of an Arbitrarily Located BD

We first determine the outage probability of a BD, conditioned on its distance from the reader  $r$ , and its angle relative to the  $x$ -axis,  $\theta$ . Allowing each BD to be served only by its nearest PB is equivalent to each PB serving only the users located to either side within an angular distance of  $\frac{\pi}{M}$ . In other words, the PB's serving region is a sector with angular width  $\frac{2\pi}{M}$ , with the PB located on the line bisecting the sector. Thus, all sectors are identical for the purpose of analysis, and we consider a representative sector (Fig. 2) in the following analysis.

For a BD located at  $(r, \theta)$ , the PB-BD and BD-reader link distances are given by  $\sqrt{d^2 + r^2 - 2dr \cos(\theta_o)}$  and  $r$ , respectively, where  $\theta_o = \theta - \theta_m$  denotes the angular offset between the BD and its nearest PB, with  $\theta_m$  representing the angle relative to the  $x$ -axis of the nearest PB with index  $m$ . The per-symbol SNR at the reader can be written as:

$$\gamma = \gamma_{eq}XY, \quad \gamma_{eq} = \frac{P\eta\beta_0^2L|b_0 - b_1|^2}{r^\delta (d^2 + r^2 - 2dr \cos(\theta_o))^{\frac{\delta}{2}} N_0} \quad (12)$$

where  $\gamma_{eq}$  can be understood as the equivalent SNR without fading, and  $X, Y \sim \Gamma\left(\kappa, \frac{1}{\kappa}\right)$  are independent and identically distributed (i.i.d.) random variables of the squared magnitude of the PB-BD and BD-reader fading coefficients, respectively. Hereafter, the terms shape parameter and Nakagami parameter are used interchangeably in reference to gamma random variables.

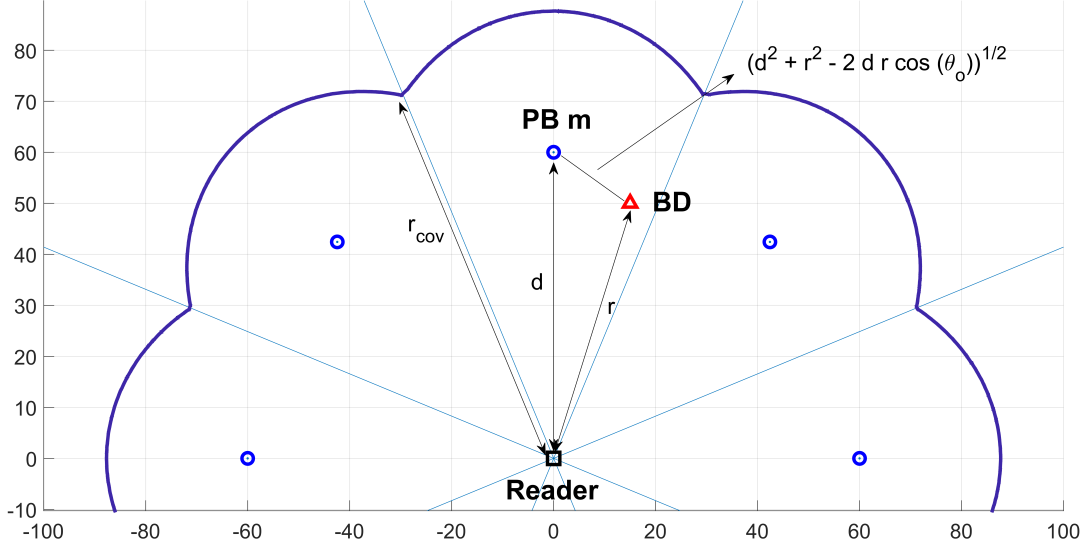


Fig. 2: Illustration of sectors for each serving PB. Also shown is an example contour within which a given QoS constraint is satisfied. The corresponding GCD is denoted by  $r_{cov}$ .

The probability density function (pdf) and cumulative distribution function (cdf) of a gamma random variable, with shape parameter  $\kappa$  and scale parameter  $\frac{1}{\kappa}$ , are given by

$$f_X(x) = \frac{\kappa^\kappa x^{\kappa-1}}{\Gamma(\kappa)} \exp(-\kappa x), \quad F_X(x) = 1 - \exp(-\kappa x) \sum_{n=0}^{\kappa-1} \frac{(\kappa x)^n}{n!}, \quad (13)$$

where, for mathematical tractability, we assume  $\kappa$  to be an integer in the cdf. The outage probability at the reader,  $P_{out}$ , is given by

$$\begin{aligned} P_{out} &= \Pr(\gamma_{eq}XY < \gamma_{th}) \quad (= F_{XY}\left(\frac{\gamma_{th}}{\gamma_{eq}}\right)) \\ &= \int_0^\infty F_X\left(\frac{\gamma_{th}}{\gamma_{eq}y}\right) f_Y(y) dy \\ &= 1 - \sum_{n=0}^{\kappa_X-1} \frac{2}{n!\Gamma(\kappa_Y)} \left(\frac{\kappa_X\kappa_Y\gamma_{th}}{\gamma_{eq}}\right)^{\frac{\kappa_Y+n}{2}} K_{\kappa_Y-n}\left(2\sqrt{\frac{\kappa_X\kappa_Y\gamma_{th}}{\gamma_{eq}}}\right), \end{aligned} \quad (14)$$

where the last expression follows from [29];  $\kappa_X$  and  $\kappa_Y$  are the shape parameters of  $X$  and  $Y$ , respectively; and  $K_\nu(\cdot)$  is the modified Bessel function of the second kind with order  $\nu$ .

### B. Solution to the PB Placement Problem

Due to the unwieldy form of  $P_{out}$ , it is difficult to solve Problem **P1** directly. Thus, we rewrite this design problem into a purely geometric form, by rearranging the outage probability

constraint into an equivalent SNR constraint (Problem **P2**):

$$\max_d \quad r_{cov} \quad (15a)$$

$$\text{s.t.} \quad \gamma_{eq} > \gamma_{eq,th} \ \&\& \ (11d), \quad (15b)$$

where  $\gamma_{eq,th}$  is the equivalent SNR threshold that is required to ensure the original outage probability constraint  $P_{out} < \varepsilon$  is met. It can be given in terms of  $\gamma_{th}$  as

$$\gamma_{eq,th} = \frac{\gamma_{th}}{F_{XY}^{-1}(\varepsilon)}, \quad (16)$$

where  $F_{XY}^{-1}$  is the inverse of the cdf of the product of  $X$  and  $Y$  from rearranging (14). Unfortunately, no closed form expression exists for  $F_{XY}^{-1}$ ; however, it is monotonic and can be empirically constructed from samples generated from the product of two gamma random variables.

Based on Problem **P2**, we present the following result on the characteristic of the coverage area, which significantly simplifies subsequent analysis. For clarity, we rewrite  $\gamma_{eq}$  in (12) as

$$\gamma_{eq} = \frac{\alpha}{r^\delta (d^2 + r^2 - 2dr \cos(\theta_o))^{\frac{\delta}{2}}}, \quad (17)$$

where  $\alpha = \frac{P\eta\beta_0^2 L |b_0 - b_1|^2}{N_0}$  denotes the distance-independent terms in the SNR.

**Proposition 1.** *For a BD deployed at distance  $r$  from the reader, the minimum equivalent SNR is obtained when the BD is located at the edge of the sector; i.e.,  $\theta_o = \frac{\pi}{M}$ .*

*Proof.* Without loss of generality, we consider a PB located on the  $x$ -axis. Then we have

$$\frac{d\gamma_{eq}}{d\theta_o} = -\frac{\alpha dr^3 \delta}{(d^2 r^2 + r^4 - 2dr^3 \cos(\theta_o))^{1+\frac{\delta}{2}}} \sin(\theta_o). \quad (18)$$

It is evident that all terms in (18) are positive for  $\theta_o \in [0, \frac{\pi}{M}]$ . For  $\theta_o \in [-\frac{\pi}{M}, 0]$ , we have  $-\sin(\theta_o) \geq 0$ . Hence, the derivative is negative in the former range and positive in the latter, and is thus an odd function passing through 0 when  $\theta_o = 0$ . As a result, minima for  $\gamma_{eq}$  must occur at the edges of the sector, i.e.,  $\theta_o = \pm \frac{\pi}{M}$ .  $\square$

Having established that the worst-case location for a BD is on the sector edge, we present our main result in the following theorem.

**Theorem 1.** *The optimal PB distance  $d^*$  when each BD is served by its nearest PB is given by*

$$d^* = \begin{cases} \left( \frac{\varsigma}{(1 - \cos^2(\frac{\pi}{M}))} \right)^{\frac{1}{4}} \cos\left(\frac{\pi}{M}\right), & M \leq \lfloor M_{th} \rfloor, \\ \left( -\frac{1}{2} \csc^2\left(\frac{\pi}{M}\right) \right)^{\frac{1}{4}} \\ \times \left( \sqrt{\varsigma^2 \cos^2\left(\frac{\pi}{M}\right) \left(9 \cos^2\left(\frac{\pi}{M}\right) - 8\right)^3 + \varsigma \left(27 \cos^4\left(\frac{\pi}{M}\right) - 36 \cos^2\left(\frac{\pi}{M}\right) + 8\right)} \right)^{\frac{1}{4}}, & M \geq \lceil M_{th} \rceil, \end{cases}$$

where  $\lfloor \cdot \rfloor$  and  $\lceil \cdot \rceil$  denote the floor and ceiling functions, respectively;  $\varsigma = \left( \frac{\alpha}{\gamma_{eq,th}} \right)^{\frac{2}{\delta}}$ ; and  $M_{th}$  is obtained at the crossover point of the two piecewise expressions above, given by

$$M_{th} = \frac{\pi}{\sec^{-1}(\omega)} \approx 12.36, \quad (19)$$

where  $\omega$  is the positive real root of the equation  $4x^6 + 2x^2 - 7 = 0$ .

*Proof.* See Appendix A. □

By straightforward evaluation of the first part to Theorem 1, we find that  $d^* = 0$  for  $M = 2$ . For  $M = 1$ , it is easy to see that any movement of the PB from the origin reduces the GCD, as the coverage area becomes irregular, thus  $d^* = 0$  also. Two additional results from Theorem 1 concern the asymptotic behavior of  $d^*$  and  $r_{cov}$  as  $M$  becomes large, which are presented next.

**Corollary 1.** *When  $M \rightarrow \infty$ , the optimal PB distance converges to*

$$d_{\infty}^* = 2\varsigma^{\frac{1}{4}}. \quad (20)$$

Moreover, the corresponding GCD,  $r_{cov}$ , as  $M \rightarrow \infty$ , can be approximated by

$$r_{cov,\infty} \approx \varsigma^{\frac{1}{4}} + \frac{1}{\sqrt{6}} \left( \left( \frac{(\sqrt{\varsigma} + (-\varsigma^{\frac{3}{2}})^{\frac{1}{3}})^2}{(-\varsigma^{\frac{3}{2}})^{\frac{1}{3}}} \right)^{\frac{1}{2}} + \left( \frac{4\varsigma + \frac{\varsigma^2}{(-\varsigma^{\frac{3}{2}})^{\frac{2}{3}}} + (-\varsigma^{\frac{3}{2}})^{\frac{2}{3}}}{\sqrt{\varsigma}} \right)^{\frac{1}{2}} \right). \quad (21)$$

Equation (20) is obtained from the expression of  $d^*$  in Theorem 1 by letting  $M \rightarrow \infty$ . Equation (21) is obtained by solving (34) in Appendix A, taking the expression of the root which represents the GCD (i.e., the smallest positive real root) with the value of  $d$  set to that obtained in (20), and then taking the limit as  $M \rightarrow \infty$ . Note that equation (21) indicates an upper bound on the achievable guaranteed coverage distance for any value of  $M$ .

#### IV. PB PLACEMENT ANALYSIS: MULTIPLE SERVING PBs

In this section, we extend the previous analysis to the case where each BD is served by multiple nearest PBs. In Section II, we have used  $\Phi$  to denote the set of indices of PBs serving

a particular BD. Hereafter, we denote the number of nearest serving PBs as  $S$  (i.e., the number of elements in  $\Phi$ ), and consider  $2 \leq S \leq M$  in this section. The outage probability expression for an arbitrarily located BD is presented first, followed by an algorithm for determining  $d^*$ .

#### A. Outage Probability of an Arbitrarily Located BD

The outage probability expression for the case where each BD performs backscatter transmission using the CW from  $S$  nearest PBs is derived similarly compared to Section III-A. The received energy at a BD from the set of serving PBs can be given by

$$E_{r,S} = \sum_{m=0}^{S-1} \left[ \frac{P\beta_0}{\left(d^2 + r^2 - 2dr \cos\left(\theta_o + \frac{2\pi m}{M}\right)\right)^{\frac{\delta}{2}}} X_m \right], \quad (22)$$

where  $X_m \sim \Gamma(\kappa_m, \frac{1}{\kappa_m})$  is the fading random variable indexed according to the PB number.

While semi-closed-form expressions [30] exist for the pdf and cdf of the sum of i.i.d. gamma random variables, a common approximation is to model the sum as another gamma random variable [31], denoted here by  $X_\Sigma$ , where given  $X_i \sim (\kappa_i, \tau_i)$ ,

$$X_\Sigma = \sum_{i=1}^n X_i \sim \Gamma(\kappa_\Sigma, \tau_\Sigma), \quad (23)$$

with

$$\kappa_\Sigma = \frac{\mu^2}{\sum_{i=1}^n \kappa_i \tau_i^2}, \quad \tau_\Sigma = \frac{\sum_{i=1}^n \kappa_i \tau_i^2}{\mu}, \quad \text{and } \mu = \sum_{i=1}^n \kappa_i \tau_i. \quad (24)$$

The combined shape parameter  $\kappa_\Sigma$  may not be integer; hence, the outage probability is given as

$$P_{out} = \Pr(\gamma < \gamma_{th}) \approx F_Z\left(\frac{\gamma_{th}}{\beta}\right), \quad (25)$$

where  $\beta$  is the equivalent path loss component of the SNR at the reader, and  $Z$  is the fading random variable associated with  $\gamma$ , comprised of the product of random variables  $X_\Sigma$  and  $Y$ .

The cdf of  $Z$  is given by

$$F_Z(z) = \frac{\pi \csc(\pi(\kappa_X - \kappa_Y))}{\Gamma(\kappa_X)\Gamma(\kappa_Y)} \left[ \Gamma(\kappa_X)(\kappa_X \kappa_Y z)^{\kappa_X} {}_1\tilde{F}_2(\kappa_X; \kappa_X + 1, \kappa_X - \kappa_Y + 1; \kappa_X \kappa_Y z) \right. \\ \left. + \Gamma(\kappa_Y)(\kappa_X \kappa_Y z)^{\kappa_Y} {}_1\tilde{F}_2(\kappa_Y; \kappa_Y + 1, \kappa_Y - \kappa_X + 1; \kappa_X \kappa_Y z) \right], \quad (26)$$

where  $\kappa_X$  and  $\kappa_Y$  are the shape parameters of  $X_\Sigma$  and  $Y$ , respectively, and  ${}_p\tilde{F}_q(\cdot; \cdot; \cdot)$  represents the regularized hypergeometric function.

### B. Solution to the PB Placement Problem

In this subsection, we outline methods to determine  $d^*$  for the multiple serving PB case. Equation (25) does not facilitate efficient solving of  $d^*$ . Therefore, we convert the multiple serving PB case to its equivalent geometric problem. The equivalent SNR threshold  $\gamma_{eq,th}$  can then be defined similarly as (16):

$$\gamma_{eq,th} = \frac{\gamma_{th}}{F_Z^{-1}(\varepsilon)}, \quad (27)$$

where  $F_Z^{-1}$  is the inverse of the cdf in (26), and can be generated empirically. Note that  $\gamma_{eq,th}$  here is an *approximation* of the exact equivalent SNR threshold, due to the approximation used in summing the fading random variables in (23).

We now present the corresponding result to Proposition 1 for  $S \geq 2$  as follows.

**Proposition 2.** *For a BD deployed at distance  $r$  from the reader, when  $S \geq 2$ , the minimum  $\gamma_{eq}$  is obtained when the BD is located at the edge of the sector, i.e.,  $\theta_o = \frac{\pi}{M}$ .*

*Proof.* When each BD is served by multiple nearby PBs, the SNR expression is derived from the summation of the received signal components from all serving PBs, and can be given by:

$$\gamma_{eq} = \sum_{m=0}^{S-1} \frac{\alpha}{\left(d^2 r^2 + r^4 - 2dr^3 \cos\left(\theta_o + \frac{2\pi m}{M}\right)\right)^{\frac{\delta}{2}}}, \quad (28)$$

The first derivative of (28) is given by

$$\frac{d\gamma_{eq}}{d\theta_o} = \sum_{m=0}^{S-1} \frac{-\alpha dr^3 \delta \sin\left(\theta_o + \frac{2\pi m}{M}\right)}{r \left(d^2 + r^2 - 2dr \cos\left(\theta_o + \frac{2\pi m}{M}\right)\right)^{\frac{\delta}{2}+1}}. \quad (29)$$

Similar to Proposition 1, it can be shown that each term in the summation of (29) is an odd function that is positive for negative  $\theta_o$  and vice versa, for any  $\delta$ . As a result, (28) is symmetric about the  $y$ -axis and is monotonically increasing for negative  $\theta_o$ , and vice versa, with maximum occurring at  $\theta_o = 0$ . Therefore, minima must occur at  $\theta_o = \pm \frac{\pi}{M}$ .  $\square$

Next, a general algorithm for determining  $d^*$  is first presented, followed by discussions on some specific values of  $S$ .

General Algorithm: First, we perform linear search to find the value(s) of  $r$  along the sector edge where (28) equals  $\gamma_{eq,th}$ . This is equivalent to obtaining  $r$  such that (25) equals  $\varepsilon$ . While we aim to obtain an expression for  $d$  in terms of  $r$ , there may be multiple values of  $r$  where equality is attained. Thus, the correct solution of  $r$  must be chosen, such that  $\gamma_{eq}$  is greater than  $\gamma_{eq,th}$  (or  $P_{out}$  is greater than  $\varepsilon$ ) up to that point. That is, the correct solution of  $r$  is the smallest



positive root of (25). If an expression exists for the correct solution of  $r$  for all  $d$ , it can be rearranged to be in the form  $d(r)$ , from which  $d^*$  can be found via algebraic manipulations; otherwise numerical search is performed. The detailed steps are provided in Algorithm 1.

---

**Algorithm 1** Computation of the optimal PB placement parameter  $d^*$

---

**Require:** Number of PBs,  $M$ ; number of serving PBs,  $S$ ; range of BD distances,  $r \in [0, r_{upper}]$ ; SNR threshold,  $\gamma_{th}$ ; outage probability threshold,  $\varepsilon$ .

- 1: Perform linear search over the range of  $r \in [0, r_{upper}]$  and compute (28) for each  $r$  to find intersection points of (28) with  $\gamma_{eq,th}$  in (27).
  - 2: For each  $r$  in Step 1, pick the smallest positive intersection point and set the resulting expression or sequence of intersection points as  $r_{cov}(d)$ .
  - 3: Compute first derivative of  $r_{cov}(d)$  numerically (or by algebraic manipulation, where an expression exists for  $r_{cov}(d)$ ) and perform linear search over  $d \in [0, \infty)$  to find the roots.
  - 4: Pick the smallest positive solution to Step 3 and set as  $d^*$ .
  - 5: **return**  $d^*$
- 

The special case of  $S = 2$ : Proposition 2 applies for any integer  $S$ ; that is, a BD located on the sector edge at distance  $r$  from the reader achieves the lowest equivalent SNR compared to any other location with distance  $r$  from the reader, regardless of the number of serving PBs. Applying this observation to the case where a BD on the sector edge is served by two nearest PBs, the achievable SNR when  $S = 2$  is twice that of  $S = 1$ . Hence, when  $S = 2$ ,

$$\gamma_{eq} = \frac{2\alpha}{r^\delta \left( d^2 + r^2 - 2dr \cos\left(\frac{\pi}{M}\right) \right)^{\frac{\delta}{2}}}. \quad (30)$$

Therefore, we can directly invoke Theorem 1 to compute  $d^*$  by setting  $\varsigma = \left( \frac{2\alpha}{\gamma_{eq,th}} \right)^{\frac{2}{\delta}}$ , where  $\gamma_{eq,th}$  refers to the equivalent SNR threshold for  $S = 2$ . Note that  $\gamma_{eq,th}$  is constant for any values of  $r$  and  $d$  only for  $S = 1$  or 2, as  $F_{XY}^{-1}$  in (16) does not depend on the path losses between individual PBs and the BD. Similarly, Corollary 1 also holds.

The special case of  $S = M$ : For  $S > 2$ , we observe that  $\gamma_{eq}$  in (27) needs to be computed for every combination of  $r$  and  $d$ , as random variable  $X_\Sigma$  accounts for the path losses between each PB and the BD, and thus closed-form expressions for  $d^*$  and  $r_{cov}$  are unlikely to exist. Here we focus on the case of  $S = M$ , as it theoretically represents the best possible coverage performance. We can exploit symmetry about the sector edge, on which the BD is located, to

deduce the total energy contribution of the PBs beyond the first and second nearest PBs. For example, the third and fourth nearest PBs have angular distance  $\frac{3\pi}{M}$  from the BD. The fifth and sixth PBs have angular distance  $\frac{5\pi}{M}$  from the BD, and so on. Therefore, the general equivalent SNR expressions for even and odd  $M$  are

$$\gamma_{eq} = 2\alpha \sum_{m=0}^{M/2-1} r^{-\delta} \left( d^2 + r^2 - 2dr \cos \left( \frac{(m+1)\pi}{M} \right) \right)^{-\frac{\delta}{2}}, \quad (31)$$

$$\gamma_{eq} = \frac{\alpha}{r^\delta (d^2 + r^2 + 2dr)^{\frac{\delta}{2}}} + 2\alpha \sum_{m=0}^{\lfloor M/2 \rfloor - 1} r^{-\delta} \left( d^2 + r^2 - 2dr \cos \left( \frac{(m+1)\pi}{M} \right) \right)^{-\frac{\delta}{2}}. \quad (32)$$

Noting the symmetry of the PBs' individual contributions,  $d^*$  may be approximated by setting  $\varsigma = \left( \frac{\chi\alpha}{\gamma_{eq,th}} \right)^{\frac{2}{\delta}}$ , where  $\chi$  is the ratio between  $\gamma_{eq}$  under  $S = M$  to  $\gamma_{eq}$  under  $S = 1$ .

## V. NUMERICAL RESULTS

In this section, we numerically evaluate the impacts of the number of PBs, the PB distance and channel parameters on the GCD of the bistatic backscatter network. Cases where each BD is served by one and multiple nearest PBs are considered. The carrier frequencies and transmit powers of all PBs are 915 MHz and 27 dBm, respectively. Unless otherwise specified, BDs are assumed to be semi-passive. We adopt  $\delta = 2.4$  as the baseline path loss exponent, which is a typical value for natural environments such as various types of forests and grassland where the nodes are located between 1-2 m above ground [32]. Where fading is considered, Nakagami fading with parameter 4 is assumed; the SNR threshold for all tags is  $\gamma_{th} = 5$  dB and the QoS constraint is  $\varepsilon = 0.05$ ; and the receive noise is  $\sigma^2 = -110$  dBm. The tag reflection efficiency is  $\eta = 0.49$  and the antenna gain is 2.1 dBi; the structural mode is set to  $A = 0.6047 + j0.5042$  for all BDs [6]; and the reflection coefficients are set to  $\{G_0, G_1\} = \{A, -\frac{A}{|A|}\}$ . BDs are attached to electrically non-conductive materials, resulting in negligible gain penalty; and the polarization mismatch loss is 0.8 for both the forward and backscatter links, to account for imperfections in BD orientations. Each symbol transmitted by a BD occurs over  $L = 20$  source samples.

### A. Optimal PB Distance and GCD Characteristics

Fig. 3(a) shows the GCD as a function of  $d$ , where  $S = 1$ , obtained via both simulation (asterisks) and Algorithm 1 (more specifically, the first two steps of Algorithm 1, which obtains the GCD for a given  $d$ ; solid lines). The simulation results are obtained using  $2 \times 10^4$  realizations of BD locations and channel coefficients. It is evident that the results obtained using Algorithm

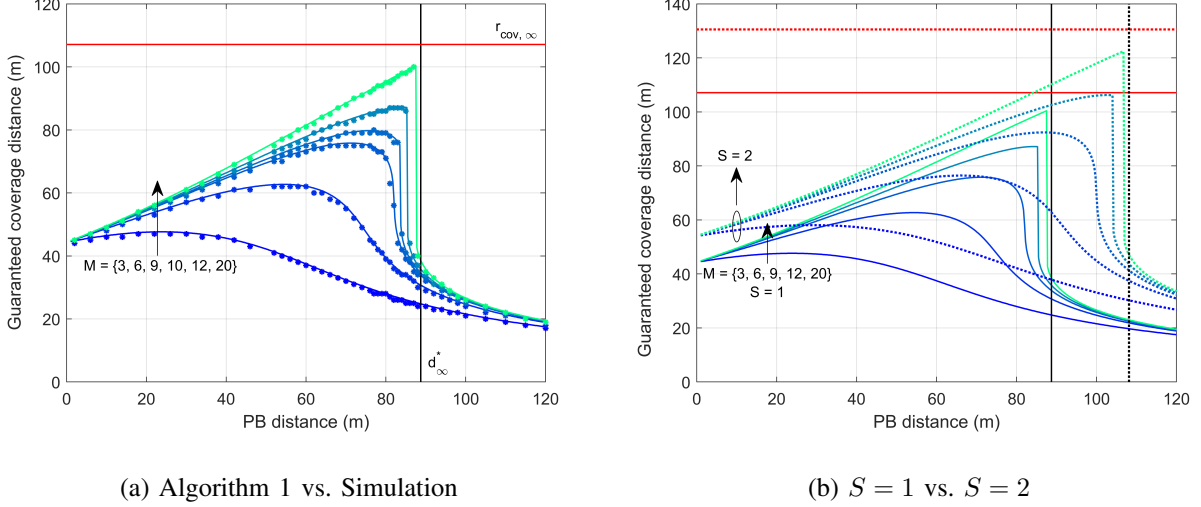


Fig. 3: Behavior of the GCD for varying  $M$ , and at various PB distances.

1 match the simulation results. The existence of an optimal PB distance is confirmed, where the optimal  $d$  that maximizes the GCD in each curve matches with  $d^*$  obtained using Theorem 1. The GCD increases with  $d$  up to a maximum, before experiencing a sharp drop. The sharpness of the drop in the GCD beyond  $d^*$  increases with the total number of PBs. Therefore, in practice, it is appropriate to deploy PBs at or at slightly less than the optimal distance, without much reduction in the GCD, but it is unwise to deploy PBs beyond the optimal distance. The upper bounds to  $d^*$  and the GCD, presented in Corollary 1, are shown using the vertical (black) and horizontal (red) lines, respectively, and it is clear that both quantities converge to their upper bounds as  $M$  increases. Hereafter, we present results obtained using Algorithm 1 only.

The characteristics of the GCD for the case of  $S = 2$  is shown in Fig. 3(b). One can observe the improvement in the GCD arising from one additional serving PB where, for example, under the case of  $M = 6$  with  $d = 50$  m, the GCD with a single serving PB is around 63 m; whereas the GCD with two serving PBs increases to 76 m, i.e., around 20% improvement. We can also see that the asymptotic GCD increases from 108 m to 130 m, i.e., a 20% improvement.

Fig. 4 shows the optimal PB distance and the corresponding maximum GCD associated with the number of deployed PBs. The benefit of increasing the number of serving PBs on the GCD diminishes as more PBs are required to serve each BD, as shown by the smaller increases in both  $d^*$  and GCD when  $S$  increases beyond 2. For a network with a small number of PBs ( $M \leq 12$ ), our results suggest to use no more than 2 serving PBs for each BD.

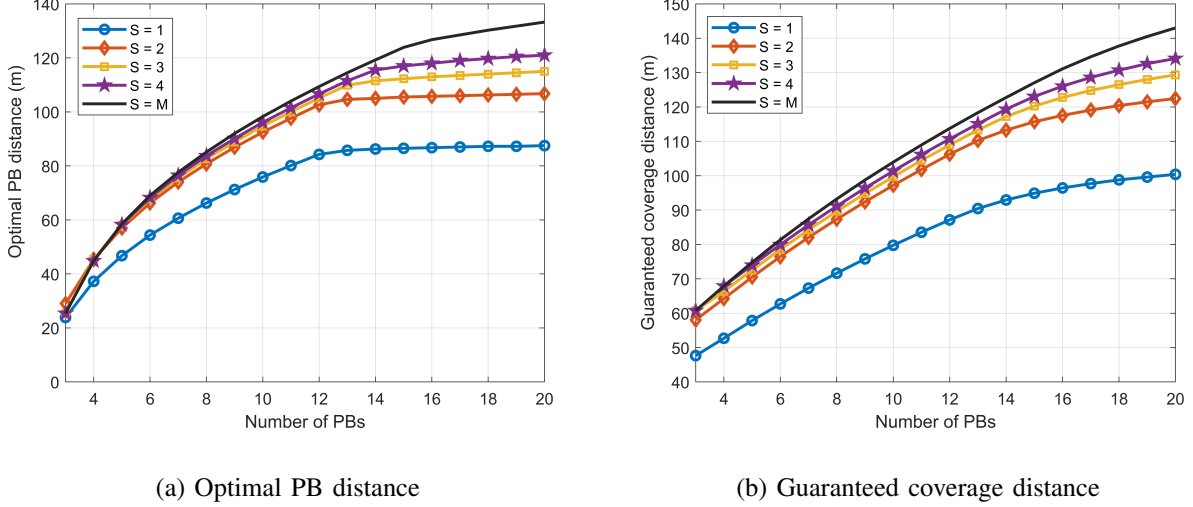


Fig. 4: Effect of the number of serving PBs on the optimal PB distance and GCD.

### B. Effect of Circuit Power Constraint

So far, our analysis and results have assumed semi-passive BDs with built-in batteries to support the circuit operation. In this subsection, we consider the case where BDs require a minimum amount of energy from the PBs in order to operate their circuits. Such a scenario may arise when passive BDs require energy harvested externally to be able to fully operate.

The addition of a circuit power constraint in the single serving PB case results in a slight modification of the SNR expression given in Section III:

$$\gamma = \left\{ \frac{P\beta_0 G_T \chi_{CT}}{(d^2 + r^2 - 2dr \cos(\frac{\pi}{M}))^{\frac{\delta}{2}}} - \xi \right\}^+ \left( \frac{\eta\beta_0 G_T \chi_{TR} |b_0 - b_1|^2 L}{r^\delta N_0} \right) XY, \quad (33)$$

where  $G_T$  and  $\chi_{CT}, \chi_{TR}$  are the antenna gains at the BD, and the polarization mismatch losses between PB-BD and BD-reader, respectively, and  $\{x\}^+ = \max\{0, x\}$ . The difference between (33) and  $\gamma$  in (12) is the inclusion of the circuit's minimum energy consumption  $\xi$ , which is subtracted from the received energy in the PB-BD link. As such, the expression in the first bracket indicates the energy available for backscattering after the circuit's energy consumption has been fulfilled, and is zero if the received energy is insufficient. This allows the shape of the joint fading distribution to be preserved with only a shift in the mean depending on  $\xi$ , thus allowing the equivalence between QoS and SNR in (16) to be similarly established. However, the addition of the constraint significantly impacts the mathematical tractability of  $d^*$ , which is

further hindered in the case of  $S \geq 2$ , where the fraction term in the first bracket becomes a summation over all  $S$  serving PBs. Thus, the solution to the PB placement problem is obtained using Algorithm 1, with numerical results presented here.

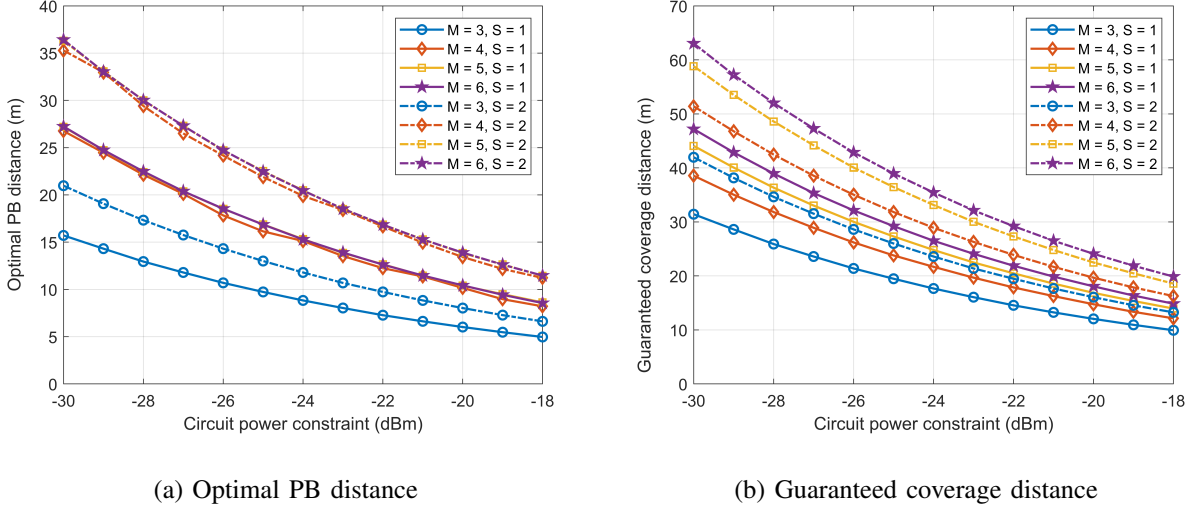


Fig. 5: Effect of BD circuit power constraint the optimal PB distance and GCD.

Fig. 5 highlights the effects of the BD circuit power constraint on the optimal PB distance. For the purpose of illustration, the transmit power of PBs is set to 35 dBm. Evidently, an increase in the circuit power constraint results in a smaller optimal PB distance and GCD, where a one order-of-magnitude increase from  $-30$  dBm to  $-20$  dBm results in around two-thirds reduction in the GCD. In addition, the optimal PB distance does not increase further when  $M > 5$ , as shown in Fig. 5(a), where the curve for  $M = 5$  completely overlaps with the curve for  $M = 6$ . Nevertheless, adding more PBs beyond  $M > 5$  still results in a small increase in the GCD, as shown in Fig. 5(b), but the small increase may not justify the cost of deploying more PBs. On the other hand, having  $S = 2$  presents a significantly improved GCD over the case of  $S = 1$ , similar to the observations in earlier numerical results.

### C. Comparisons with Alternative Placement Schemes

The optimality of the single-tier PB placement scheme adopted in this work may be intuitive to understand for a small number of PBs. Nevertheless, one may expect that a two-tier symmetric scheme should outperform the single-tier scheme when  $M$  is large. Therefore, it is important to compare the performance between the single-tier and two-tier schemes. Fig. 6 compares the

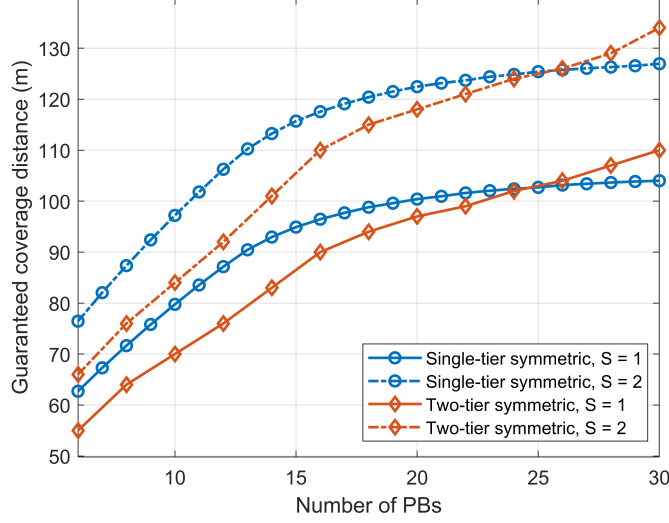


Fig. 6: Comparison of the GCD between the single-tier symmetric and two-tier symmetric placement schemes for  $S = 1$  and  $S = 2$ .

maximum achievable GCD for the single-tier symmetric scheme studied in this paper against a two-tier symmetric scheme. Under the two-tier scheme, each tier has at least 3 PBs. Hence, the number of PBs in the inner and outer tiers are  $M_1 = \{3, \dots, M - 3\}$  and  $M_2 = M - M_1$ , respectively, where  $M \geq 6$ . The distance of the inner tier is set to  $d^*$  from the single-tier scheme (from Theorem 1) when  $M_1$  PBs are deployed; while the distance of the outer tier is numerically optimized over a range within the vicinity of this value. At each outer tier distance, the rotation offset of the second-tier PBs relative to the positive  $x$ -axis is varied between  $[0, \frac{\pi}{M_2}]$ . For each value of  $M$ , the largest GCD achieved by any combination of  $M_1$ ,  $M_2$ , the outer tier distance and rotation offset is numerically obtained and shown in Fig. 6. One can observe that for both  $S = 1$  and  $S = 2$ , single-tier outperforms two-tier up to at least  $M = 24$ , which is already a relatively large number of PBs. Beyond this threshold, the two-tier scheme has a performance advantage in cases where the optimal placement allocates more PBs in the outer tier than the inner tier. However, the computation of an optimal two-tier placement requires much higher complexity than Algorithm 1 due to the additional variables involved. Moreover, it is usually not wise in practice to deploy a very large number of PBs in multiple tiers surrounding a single reader in order to grow the coverage area, as the gains in coverage area are limited with more added PBs. When wide-area coverage is concerned, a more efficient network deployment strategy (beyond

the scope of this work) is the use of multiple readers, each of which is surrounded by a relatively small number of PBs placed according to the single-tier scheme. Thus, the single-tier scheme balances good performance with reasonable deployment costs.

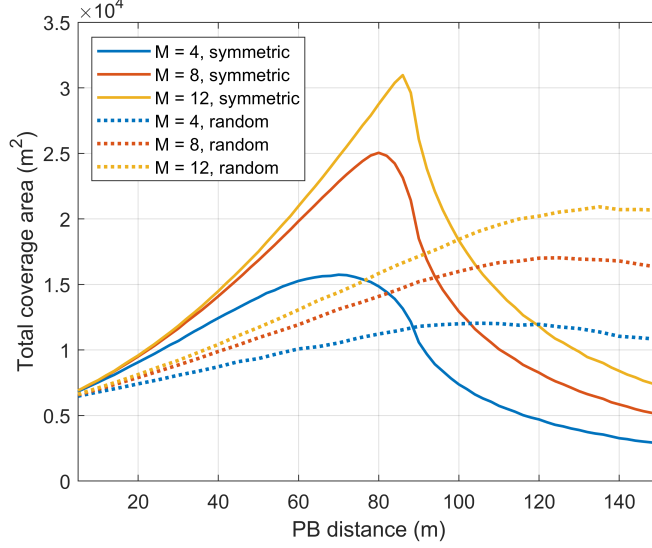


Fig. 7: Comparison of the total coverage area between the symmetric and random PB placement schemes, where each PB is served by its nearest PB (i.e.,  $S = 1$ ).

Finally, we examine the performance comparison with a random placement scheme, which is typically considered in the literature as a useful benchmark. Note that the GCD is no longer a suitable metric for random placement, which may result in scattered ‘uncovered’ regions closer to the reader while regions further away from the reader are covered. For fair comparison, we use the total coverage area as the metric. Note that for the symmetric placement scheme, the total coverage area includes the additional ‘covered’ regions beyond the GCD. Fig. 7 presents the numerically computed total coverage areas for both the symmetric and random placement schemes. The PB distance  $d$  for the symmetric placement scheme is the same as defined previously in this paper. The PB distance  $d$  for the random placement scheme denotes the maximum distance for PB placement, where  $M$  PBs are randomly placed according to a uniform distribution in a disk region of radius  $d$  centered at the reader. Hence, the  $x$ -axis in Fig. 7 refers to different quantities for the two schemes. It is clear that when all areas satisfying the SNR threshold are accounted for, the symmetric placement scheme outperforms the random scheme in terms of the maximum achievable total coverage area (i.e., the total coverage area achieved

at the optimal distance parameter value), by 25-35% for the values of  $M$  considered.

## VI. CONCLUSION

In this paper, a single-tier symmetric PB placement strategy for a bistatic backscatter network was studied, with the objective of maximizing the guaranteed coverage distance. Expressions for the outage probability were derived for the cases where a BD is served by one or multiple nearest PBs. In addition, closed-form expressions for the optimal PB placement distance were shown to be attainable for the cases of serving with one and two nearest PBs. Notably, when the number of PBs in the network is small, the use of two nearest PBs as serving PBs is a favorable choice. Moreover, the advantages of the single-tier symmetric placement scheme over other schemes, such as the two-tier symmetric and random schemes, were also demonstrated. This paper presents an introductory study into the efficient infrastructure deployment in bistatic backscatter networks. Future work can extend towards optimal placement of both PBs and readers to cover larger geographical areas.

## APPENDIX A

### PROOF OF THEOREM 1

We wish to solve the equation  $\gamma_{eq} = \gamma_{eq,th}$ , and maximize the resulting expression to obtain  $d^*$ . It is already established in Proposition 1 that for a BD at distance  $r$  from the reader, the location where it achieves the lowest SNR must lie on the sector edge; that is,  $\theta_o = \frac{\pi}{M}$ . The equation to be solved becomes a quartic polynomial by rearranging  $\gamma_{eq}$  in (12):

$$f(r) = r^4 - 2dr^3 \cos\left(\frac{\pi}{M}\right) + d^2r^2 - \varsigma, \quad (34)$$

where we have defined  $\varsigma = \left(\frac{\alpha}{\gamma_{eq,th}}\right)^{\frac{2}{\delta}}$ . Equation (34) is analogous to a path loss function, and has the same roots as the equation  $\gamma = \gamma_{th}$ . Hereafter, we denote  $\cos\left(\frac{\pi}{M}\right)$  as  $\Theta$  for compactness. We first present the following result, which aids the remainder of the proof.

**Lemma 1.** *The equivalent SNR of a BD on the sector edge is monotonically decreasing as  $r$  increases, for  $M \leq 9$ . The monotonicity condition does not hold for  $M \geq 10$ .*

*Proof.* We consider the domain  $r \in [0, \infty)$ . The roots of the first derivative of (34) with respect to  $r$  tell us the segments on the sector edge where the SNR is increasing or decreasing:

$$\frac{d\varsigma}{dr} = 4r^3 - 6dr^2\Theta + 2d^2r. \quad (35)$$



Equation (35) tends to  $\infty$  as  $r$  increases, and can be simplified to a (convex) quadratic  $4r^2 - 6dr\Theta + 2d^2$  by observing that there is a zero root. The discriminant of this quadratic,  $9d^2\Theta^2 - 8d^2$ , is less than zero for all  $d$  when  $\Theta < \frac{7}{9}$ ; taking the floor of the resulting inequality solution gives  $M \leq 9$ . When this is true, (35) has two complex roots in addition to the zero root, and is hence positive for all  $r > 0$ . It follows that the discriminant must be positive for some  $d$ , when  $M \geq 10$ . As the path loss function in (34) is an inverted form of the SNR, the SNR is non-increasing for  $M \leq 9$ , and non-monotonic otherwise.  $\square$

Deferring the case where both non-zero roots of (35) are real and equal to the sequel, we can observe from Lemma 1 that there are two cases regarding the two roots in question:

- If both real, then along the sector edge,  $\gamma_{eq} > \gamma_{eq,th}$  for small  $r$ , then  $\gamma_{eq} < \gamma_{eq,th}$  for some time where  $r \approx d$ , and then  $\gamma_{eq} > \gamma_{eq,th}$  as  $r \rightarrow \infty$ . In this case, (34) has three positive real roots, where  $f(r) > 0$  between the first and second roots (corresponding to a coverage gap); and  $r_{cov}$  is equal to the smallest positive real root.
- If both complex, then the SNR is monotonically decreasing for all  $r$ ; and  $r_{cov}$  is the single positive real root of (34).

Let  $r_{max}$  be the largest positive real root to (34). For  $M \leq 9$ , where only one positive real root exists for  $f(r)$ ,  $r_{cov}$  is equal to  $r_{max}$ . For  $M \geq 10$ , depending on  $M$  and  $\gamma_{eq,th}$ ,  $r_{cov}$  may correspond to a smaller root, since continuous coverage on the sector edge is not guaranteed.

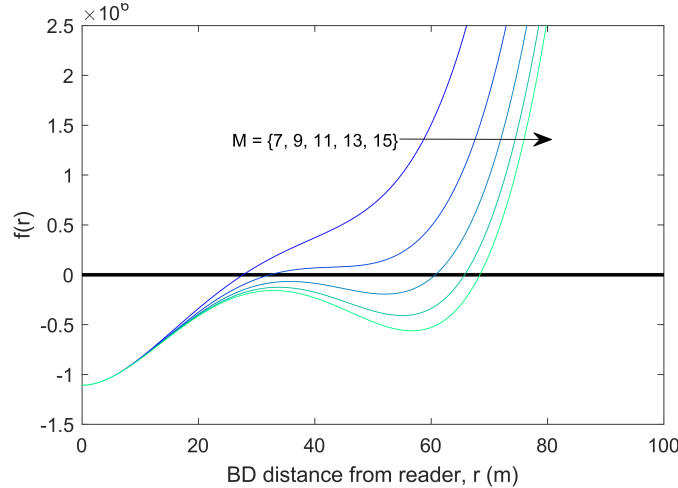


Fig. 8: Behavior of path loss function in (34) as  $M$  increases.

The behavior of  $f(r)$  is illustrated in Fig. 8 for representative values of  $d$ ,  $\varsigma$  and  $M$ . Note

that the remaining root is located in the negative  $x$ -axis. The occurrence of three positive roots depends on the value of  $\gamma_{th}$ , which translates to a vertical shift in the path loss function in (34). It is evident that (34) is non-decreasing for  $M \leq 9$ , and that the coverage gap behavior, occurring when three positive real roots exist, becomes apparent for  $M \geq 11$  and certain values of  $\varsigma$ .

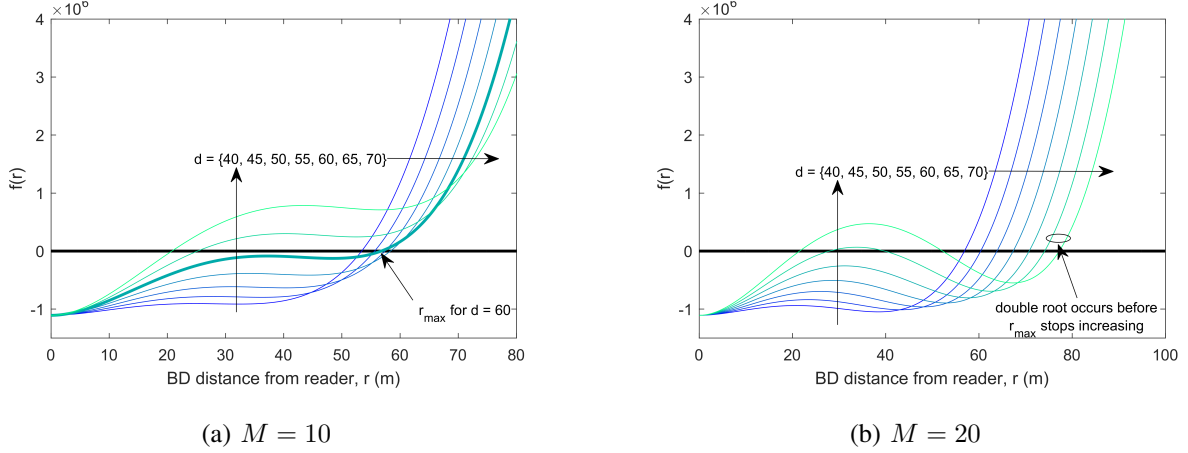


Fig. 9: Behavior of path loss function in (34) when varying  $d$ .

We also illustrate a situation where  $d$  is varied holding  $M$  constant in Fig. 9, for  $d$  between 40 and 70 in steps of 5, and a small and large value of  $M$ . It is clear that for the small- $M$  case,  $r_{max}$  begins to decrease between  $d = 55$  and 60, despite the two other real roots not having occurred. The curve for  $d = 60$  is shown in bold to illustrate the reduction in  $r_{max}$ . In the large- $M$  case,  $r_{max}$  continually increases as the other roots appear.

These observations are sufficient to imply the existence of two regimes depending on  $M$ , and that there are different expressions for  $d^*$  under each regime. The boundary can be thought of as a differentiator between two cases as  $d$  is increased:

- **Case (a):** Either  $r_{max}$  stops increasing before the occurrence of a real double root in  $f(r)$  (which includes the case where  $M \leq 9$ , where the double roots are complex), in which case the largest feasible  $r$ , i.e.,  $r_{max}$ , determines  $d^*$ ; or
- **Case (b):**  $r_{max}$  stops increasing after the occurrence of a real double root in  $f(r)$ , in which case  $d^*$  is equal to the smallest value of  $d$  where the double root first occurs.

These are the only two possibilities; therefore, such a boundary exists.

Ideally, to obtain  $d^*$ , one first determines the smallest positive real root of (34), and then finds  $d$  which maximizes the root expression. However, due to the unwieldy form of the exact roots of quartic polynomials, we take an alternative approach. In **Case (a)**,  $r_{max}$  is simply the largest feasible value of  $r$ , regardless of whether a coverage gap exists or not. Therefore, we determine  $d^*$  by considering (34) as a function of  $d$ , which is a convex quadratic function:

$$f(d) = r^2 d^2 - 2r^3 \Theta d + (r^4 - \varsigma). \quad (36)$$

For a given  $r$ , the existence of real roots to  $f(d)$  effectively indicates that the value of  $r$  is feasible. In other words, if a BD lies on the sector edge at distance  $r$  from the reader, then there exists a range of  $d$  within which the equivalent SNR constraint can be satisfied for that BD; that range of  $d$  is between the two roots of (36). Using this observation, we first find  $r_{max}$  by using the fact that  $f(d)$  has a double root when  $r = r_{max}$ ; that is, the double root is the point where only one value of  $d$  makes  $r$  just feasible. By completing the square on (36), we require

$$r_{max}^4 - \varsigma - \frac{4r_{max}^6 \Theta^2}{4r_{max}^2} = 0 \Rightarrow r_{max} = \left( \frac{\varsigma}{1 - \Theta^2} \right)^{\frac{1}{4}}. \quad (37)$$

The corresponding solution for  $d$  can then be found by computing the vertex of the quadratic in (36), which equates to  $\frac{2r_{max}^3 \Theta}{2r_{max}^2} = r_{max} \Theta$ .

From the previous discussion on **Case (a)**, we note that  $r_{max}$  in (37) is valid up to some threshold for  $M$ , denoted by  $M_{th}$ , where  $M_{th} > 9$ . In other words,  $M_{th}$  is the point where  $r_{cov}$  switches from the largest positive real root to the smallest positive real root of (34). This gives the first part to Theorem 1, and is summarized in Lemma 2 below.

**Lemma 2.** *For  $M \leq M_{th}$ , the optimal PB deployment distance  $d^*$  is given by*

$$d^* = \left( \frac{\varsigma}{1 - \Theta^2} \right)^{\frac{1}{4}} \Theta. \quad (38)$$

Note that as  $M \rightarrow \infty$ ,  $d^*$  in (38) approaches infinity, which is not possible even with large  $M$  when a single serving PB is assumed. This confirms the existence of a boundary between the small- $M$  regime and the large- $M$  regime. Now we are required to determine  $M_{th}$ . In light of this, we examine **Case (b)**, where we revisit the case where (35) takes on a double root, which only becomes possible when  $M \geq 10$ . In other words, there exists a point where as  $d$  increases, (34) switches from having one positive real root to first a single root plus a double root, and then three positive real roots. Taking advantage of this behavior, we provide the following closed-form result for the value of  $d$  at which the double root occurs.

**Lemma 3.** For  $M \geq 10$ , the distance  $d'$  at which (34) admits a real double root is given by

$$d' = \left( -\frac{1}{2} \csc^2 \left( \frac{\pi}{M} \right) \left( \sqrt{\varsigma^2 \Theta^2 (9\Theta^2 - 8)^3} + \varsigma (27\Theta^4 - 36\Theta^2 + 8) \right) \right)^{\frac{1}{4}}. \quad (39)$$

*Proof.* See Appendix B.  $\square$

It can be shown that (39) converges to a finite value as  $M \rightarrow \infty$ . As such, we are now required to find the intersection of the two expressions in Lemmas 2 and 3. This allows us to determine  $M_{th}$  where the correct  $d^*$  switches from (38) to (39); that is, the value of  $d$  where the double root in (34) occurs before  $r_{max}$  stops increasing. The value of  $M_{th}$  can be obtained using standard mathematical packages. It follows that the correct value of  $d^*$  for a given  $M$  is the smaller of the expressions in Lemmas 1 and 3. This completes the proof.

## APPENDIX B

### PROOF OF LEMMA 3

We derive the closed-form expression of  $d'$ , which holds when (34) admits a real double root. By rearranging the coefficients of the depressed quartic equation in [33], for a quartic equation of the form  $a_4x^4 + a_3x^3 + a_2x^2 + a_1x + a_0 = 0$ , the conditions for a double root to occur are:

$$\Delta = 0, \quad (40)$$

$$8a_4a_2 - 3a_3^2 < 0, \quad (41)$$

$$64a_4^3a_0 - 16a_4^2a_3a_1 - 16a_4^2a_2^2 + 16a_4a_3^2a_2 - 3a_3^4 < 0, \quad (42)$$

$$a_2^2 + 12a_4a_0 - 3a_3a_1 \neq 0, \quad (43)$$

where  $\Delta$  is the discriminant. When  $a_1 = 0$ ,

$$\begin{aligned} \Delta &= 256a_4^3a_0^3 - 128a_4^2a_2^2a_0^2 + 144a_4a_3^2a_2a_0^2 + 16a_4a_2^4a_0 - 27a_3^4a_0^2 - 4a_3^2a_2^3a_0 \\ &= (16\varsigma\Theta^2 - 16\varsigma) d^8 + (576\varsigma^2\Theta^2 - 128\varsigma^2 - 432\varsigma^2\Theta^4) d^4 - 256\varsigma^3. \end{aligned} \quad (44)$$

Equation (44) is quadratic with respect to  $d^4$ . Solving (44) and taking the positive root yields the result in (39). The negative root is given by

$$(d^4)_- = \left( \frac{1}{4} \left( 9\varsigma + 27\varsigma \cos \left( \frac{2\pi}{M} \right) + 2 \left( \varsigma + \sqrt{\varsigma^2 \Theta^2 (9\Theta^2 - 8)^3} \right) \csc^2 \left( \frac{\pi}{M} \right) \right) \right)^{\frac{1}{4}}. \quad (45)$$

$(d^4)_-$  tends to infinity as  $M$  grows large, and therefore cannot be the correct solution. It can be shown that (45) upper bounds (38) for  $M \geq 10$ , implying that no boundary exists between

the small- $M$  and large- $M$  regimes, contradicting previous observations. We check that the other conditions are satisfied for the positive root. Inequality (41) is independent of  $d$  and simplifies to  $M \geq 6$ , which is already true since it is assumed that  $M \geq 10$ . Rearranging (42) gives

$$d^4 > \frac{4\zeta}{1 + 3\Theta^4 - 4\Theta^2}, \quad (46)$$

where the RHS is always negative. Inequation (43) simplifies to  $d^4 \neq 12\zeta$ , which is the condition required for a triple root to occur. However, a triple root can only occur when the discriminant in Lemma 1 is zero, which is not possible for an integer value of  $M$ . Therefore, the positive root in (39) is the correct solution, as long as (42) and (43) are not violated.

## REFERENCES

- [1] G. Vannucci, A. Bletsas, and D. Leigh, "A software-defined radio system for backscatter sensor networks," *IEEE Trans. Wireless Commun.*, vol. 7, no. 6, pp. 2170–2179, Jun. 2008.
- [2] A. Bletsas, A. G. Dimitriou, and J. N. Sahalos, "Improving backscatter radio tag efficiency," *IEEE Trans. Microw. Theory Techn.*, vol. 58, no. 6, pp. 1502–1509, Jun. 2010.
- [3] C. Boyer and S. Roy, "Coded QAM backscatter modulation for RFID," *IEEE Trans. Commun.*, vol. 60, no. 7, pp. 1925–1934, Jul. 2012.
- [4] R. Sadr, J. Gevargiz, R. Lee, M. Manteghi, G. Oliver, M. Collender, C. Jones, and H. Syed, "RFID systems using distributed exciter network," Mar. 12 2013, US Patent 8,395,482.
- [5] J. D. Griffin and G. D. Durgin, "Complete link budgets for backscatter-radio and RFID systems," *IEEE Antennas Propag. Mag.*, vol. 51, no. 2, pp. 11–25, 2009.
- [6] J. Kimionis, A. Bletsas, and J. N. Sahalos, "Increased range bistatic scatter radio," *IEEE Trans. Commun.*, vol. 62, no. 3, pp. 1091–1104, Mar. 2014.
- [7] N. Fasarakis-Hilliard, P. N. Alevizos, and A. Bletsas, "Coherent detection and channel coding for bistatic scatter radio sensor networking," *IEEE Trans. Commun.*, vol. 63, no. 5, pp. 1798–1810, May 2015.
- [8] Z. Shen, A. Athalye, and P. M. Djuric, "Phase cancellation in backscatter-based tag-to-tag communication systems," *IEEE Internet Things J.*, vol. 3, no. 6, pp. 959–970, Dec. 2016.
- [9] P. N. Alevizos, A. Bletsas, and G. N. Karystinos, "Noncoherent short packet detection and decoding for scatter radio sensor networking," *IEEE Trans. Commun.*, vol. 65, no. 5, pp. 2128–2140, May 2017.
- [10] G. Zhu, S. Ko, and K. Huang, "Inference from randomized transmissions by many backscatter sensors," *IEEE Trans. Wireless Commun.*, vol. 17, no. 5, pp. 3111–3127, May 2018.
- [11] K. Han and K. Huang, "Wirelessly powered backscatter communication networks: Modeling, coverage, and capacity," *IEEE Trans. Wireless Commun.*, vol. 16, no. 4, pp. 2548–2561, Apr. 2017.
- [12] P. N. Alevizos, K. Tountas, and A. Bletsas, "Multistatic scatter radio sensor networks for extended coverage," *IEEE Trans. Wireless Commun.*, vol. 17, no. 7, pp. 4522–4535, Jul. 2018.
- [13] M. Bacha, B. Clerckx, and K. Huang, "Backscatter communications for the internet of things: A stochastic geometry approach. [Online]. Available: <https://arxiv.org/pdf/1711.07277.pdf>
- [14] X. Cheng, D.-Z. Du, L. Wang, and B. Xu, "Relay sensor placement in wireless sensor networks," *Wireless Netw.*, vol. 14, no. 3, pp. 347–355, Jun. 2008.

- [15] M. Minelli, M. Ma, M. Coupechoux, J. Kelif, M. Sigelle, and P. Godlewski, "Optimal relay placement in cellular networks," *IEEE Trans. Wireless Commun.*, vol. 13, no. 2, pp. 998–1009, Feb. 2014.
- [16] D. Yang, X. Fang, G. Xue, and J. Tang, "Relay station placement for cooperative communications in WiMAX networks," in *Proc. IEEE Global Commun. Conf. (GLOBECOM)*, Dec. 2010, pp. 1–5.
- [17] E. L. Lloyd and G. Xue, "Relay node placement in wireless sensor networks," *IEEE Trans. Comput.*, vol. 56, no. 1, pp. 134–138, Jan 2007.
- [18] C. Zhong, X. Chen, Z. Zhang, and G. K. Karagiannidis, "Wireless-powered communications: Performance analysis and optimization," *IEEE Trans. Commun.*, vol. 63, no. 12, pp. 5178–5190, Dec. 2015.
- [19] H. Ju and R. Zhang, "Throughput maximization in wireless powered communication networks," *IEEE Trans. Wireless Commun.*, vol. 13, no. 1, pp. 418–428, Jan. 2014.
- [20] J. Guo, X. Zhou, and S. Durrani, "Wireless power transfer via mmWave power beacons with directional beamforming," *IEEE Wireless Commun. Lett.*, vol. 8, no. 1, pp. 17–20, Feb. 2019.
- [21] H. Tabassum and E. Hossain, "On the deployment of energy sources in wireless-powered cellular networks," *IEEE Trans. Commun.*, vol. 63, no. 9, pp. 3391–3404, Sep. 2015.
- [22] S. Bi and R. Zhang, "Placement optimization of energy and information access points in wireless powered communication networks," *IEEE Trans. Wireless Commun.*, vol. 15, no. 3, pp. 2351–2364, Mar. 2016.
- [23] K. Huang and V. K. N. Lau, "Enabling wireless power transfer in cellular networks: Architecture, modeling and deployment," *IEEE Trans. Wireless Commun.*, vol. 13, no. 2, pp. 902–912, Feb. 2014.
- [24] Z. Wang, L. Duan, and R. Zhang, "Adaptively directional wireless power transfer for large-scale sensor networks," *IEEE J. Sel. Areas Commun.*, vol. 34, no. 5, pp. 1785–1800, May 2016.
- [25] K. Liang, L. Zhao, G. Zheng, and H. Chen, "Non-uniform deployment of power beacons in wireless powered communication networks," *IEEE Trans. Wireless Commun.*, vol. 18, no. 3, pp. 1887–1899, Mar. 2019.
- [26] C. Zhang and G. Zhao, "On the deployment of distributed antennas of power beacon in wireless power transfer," *IEEE Access*, vol. 6, pp. 7489–7502, 2018.
- [27] O. M. Rosabal, O. L. A. López, H. Alves, S. Montejo-Sánchez, and M. Latva-aho, "On the optimal deployment of power beacons for massive wireless energy transfer," *IEEE Internet Things J.*, pp. 1–1, 2020.
- [28] M. Vestakis, P. N. Alevizos, G. Vougioukas, and A. Bletsas, "Multistatic narrowband localization in backscatter sensor networks," in *Proc. Int. Workshop Signal Process. Advances in Wireless Commun. (SPAWC)*, 2018, pp. 1–5.
- [29] P. Van, H. N. Le, M. N. Le, and D. Ha, "Performance analysis in wireless power transfer system over Nakagami fading channels," in *Proc. Int. Conf. Electron. Info. Commun. (ICEIC)*, Jan. 2016, pp. 1–4.
- [30] P. G. Moschopoulos, "The distribution of the sum of independent gamma random variables," *Ann. Inst. Statist. Math.*, vol. 37, no. Part A, pp. 541–544, 1985.
- [31] S. Covo and A. Elalouf, "A novel single-gamma approximation to the sum of independent gamma variables, and a generalization to infinitely divisible distributions," *Electron. J. Statist.*, vol. 8, no. 1, pp. 894–926, 2014.
- [32] J. A. Gay-Fernández and I. Cuiñas, "Peer to peer wireless propagation measurements and path-loss modeling in vegetated environments," *IEEE Trans. Antennas Propag.*, vol. 61, no. 6, pp. 3302–3311, 2013.
- [33] E. L. Rees, "Graphical discussion of the roots of a quartic equation," *Amer. Math. Monthly*, vol. 29, no. 2, pp. 51–55, 1922. [Online]. Available: <http://www.jstor.org/stable/2972804>